International Journal of Quantum Technologies

PRIME OPEN ACCESS

Volume 1, Issue 2

Research Article

Date of Submission: 30 May, 2025
Date of Acceptance: 10 July, 2025
Date of Publication: 21 July, 2025

Fabry-Perot Cavity Based Selective Emitters Intended for Medium Grade Waste Heat Sources and Spectral Response of Silicon, Germanium and Gallium Arsenide Converter Cells for Thermophotovoltaic Systems

Maria Masood*

Independent Researcher, Germany

***Corresponding Author:**
Maria Masood, Independent Researcher, Germany.

Citation: Masood, M. (2025). Fabry-Perot Cavity Based Selective Emitters Intended for Medium Grade Waste Heat Sources and Spectral Response of Silicon, Germanium and Gallium Arsenide Converter Cells for Thermophotovoltaic Systems. *Int J Quantum Technol, 1*(2), 01-14.

Abstract
This research investigates the design and performance of Fabry-Perot cavity-based selective emitters for medium-grade waste heat sources focusing on their application in thermophotovoltaic (TPV) systems. A series of metal-insulator-metal multilayer stacks, comprising various metals (such as aluminum, tungsten, gold, silver, and titanium nitride) and dielectrics, were analyzed, using the transfer matrix method (TMM) to determine their absorption and emission spectra. The goal was to optimize the selective emission properties for TPV systems using Silicon, Germanium and Gallium Arsenide converter cells. Results show that certain MIM structures, particularly those based on aluminum and silica, offer narrow absorption peaks that align with the bandgap wavelengths of these converter cells, maximizing efficiency while minimizing thermal losses. The study further explores the spectral response of the converter cells and the effect of material thickness, angle of incidence and polarization on the absorption spectra. This work demonstrates that tailored selective emitters can significantly affect the performance of TPV systems, contributing to enhanced energy efficiency in medium-grade heat recovery applications.

Keywords: Transfer Matrix Method, Fabry-Perot Cavity, Medium-Grade Heat Recovery, Gallium Arsenide

Introduction
In this research, planar multilayer Metal Insulator Metal (MIM) stacks are designed and studied as potential selective emitters for a TPV system. A MIM multilayer stack, is a Fabry-Perot cavity consisting of an insulator coating on the top, below which is a thin metal layer, followed by an insulator layer, and then a thick metal layer at the bottom. This cavity is considered on top of a thick Silicon substrate.

INSULATOR
METAL
INSULATOR
METAL
SUBSTRATE

Table 1: A MIM Multilayer Stack

A TPV system, mainly consists of an emitter, which absorbs heat from a heat source and emits radiation. This radiation is sent to a converter cell, which converts this radiation to electricity. This heat may come from various sources. The converter cell is a photovoltaic (PV) cell, with a bandgap energy, which is the distance between its conduction band and valence band. Different materials may have different bandgap energies corresponding to different bandgap wavelengths. Three such materials are as listed in Table 2.

Material	Bandgap Energy (eV)	Bandgap Wavelength (nm)
Si	1.1	1100
Ge	0.75	1840
GaAs	1.42	870

Table 2: Bandgap Energy and Wavelength of Few Materials Under Consideration

The spectral mismatch between the output of an emitter and the bandgap of a converter cell is the main obstacle in making efficient TPV systems. The broader the emission spectrum of the emitter, the more radiation is lost as heat. The spectral control of the emissivity of the emitter has been found to be realized using numerous methods [1].

Ideally, a selective emitter emits radiation only around a designed wavelength that, in TPV system, matches the bandgap wavelength of the PV cell [2]. It is desired that most of the output radiation of the selective emitter is below the bandgap wavelength of the converter cell. Low bandgap converter cells have their bandgap resonance at a higher wavelength allowing more radiation to fall under the 'useful' radiation category. A selective emitter is integral to prevent damage to the PV cell due to overheating, together with the installation of reflectors and heat sinks at the back of the PV cell.

This research is particularly for medium-grade heat sources, which can originate from various sources [3]. Medium-grade heat refers to heat energy that is typically generated at temperatures ranging from 500K to 900K. By efficiently capturing and utilizing medium-grade heat, industries and communities can improve energy efficiency and reduce overall energy consumption and greenhouse gas emissions.

Understanding the absorptivity and emissivity through Kirchhoff's law is fundamental in the study of selective emitters. In thermal equilibrium, the law ensures that the emission properties of a material can be accurately predicted by its absorption spectrum. This principle simplifies the analysis of emitters since the complex task of the direct emissivity measurements can be circumvented by studying the absorption characteristics.

Choice of Materials for the Selective Emitters

MIM multilayer stacks with different thicknesses and materials were studied using the transfer matrix method (TMM) as candidates for selective emitters. The TMM algorithm facilitates this process by providing a precise model for the interaction of light with multilayer structures, enabling detailed absorption spectra to be generated and analyzed. In the TMM simulations the thicknesses and refractive indices for each layer is suggested as input and the output is the reflectance and transmittance of the stack, from which we may calculate its absorption [4,5].

The response of few multilayers was studied around the bandgap wavelength of Germanium (Ge), as an example, to observe how variations in the choice of the metal affects the absorption peak width, position and intensity. Five metals were considered – Tungsten (W), Aluminum (Al), Gold (Au), Silver (Ag) and Titanium Nitride (TiN). The dielectric considered in this section was Hafnia. The refractive indices of the metals in this section were taken as a function of wavelength from the database for W, for Al, for Au and for Ag [6-8]. In the case of TiN, the refractive index was calculated after extracting plasmonic parameters like the damping coefficient and the plasma frequency obtained from fitting the reflectance of a thin TiN layer on Silicon substrate to a Drude Lorentz Model in RefFIT software. The refractive index for the dielectric Hafnia was taken constant as 1.8981.

The considered thicknesses of these multilayer stacks are as mentioned in Table 3. Normal incidence and unpolarized light were considered.

	TiN/Hafnia	Ag/Hafnia	Au/Hafnia	Al/Hafnia	W/Hafnia
Dielectric	90nm	90nm	90nm	90nm	90nm
Metal	10nm	10nm	10nm	10nm	10nm
Dielectric	250nm	417nm	415nm	450nm	275nm
Metal	400nm	400nm	400nm	400nm	400nm
Substrate	Silicon Substrate	Silicon Substrate	Silicon Substrate	Silicon Substrate	Silicon Substrate

Table 3: Multilayer Selective Emitters Based on Different Materials and Thicknesses

With reference to Figure 1, the peak width is different for different metals. The MIM stacks made of Ag and Au with Hafnia as the dielectric were found to be the best. As desired, they were found to have quite a narrow peak around the bandgap wavelength of Ge. This means the radiation which is not useful is not sent to the PV cell, and hence enhanced recombination of charge carriers in the cell. The absorption peak-width is broad in the case of TiN/Hafnia and W/Hafnia multilayers, with high absorption intensity.

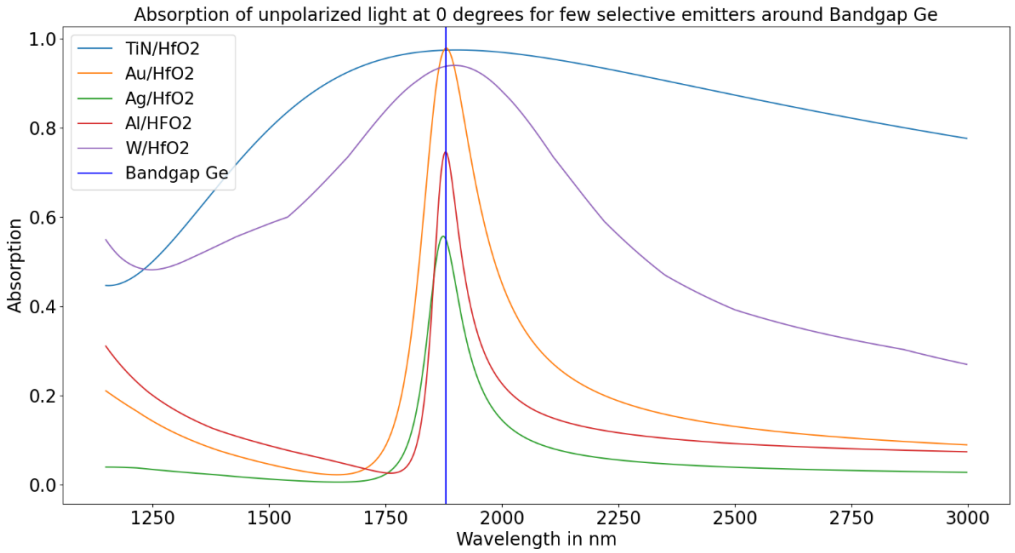

Figure 1: Comparison of Absorption of Different Multilayer Selective Emitter Stacks Described in Table 3

Al/Silica Multilayers as Selective Emitters

Having exhaustively analyzed various MIM multilayer stacks as potential candidates for selective emitters, three Al/ Silica MIM multilayer stacks with different thicknesses were studied in detail with absorption peaks around the bandgap wavelengths of three converter cells. As shown in Table 4 and Figure 2. The refractive index for the dielectric Silica was taken as 1.4585.

	SELECTIVE EMITTER 1	SELECTIVE EMITTER 2	SELECTIVE EMITTER 3
Silica	90 nm	120 nm	90 nm
Aluminum	10 nm	5 nm	10 nm
Silica	330 nm	80 nm	585 nm
Aluminum	400 nm	150 nm	400 nm
Substrate	Silicon Substrate	Silicon Substrate	Silicon Substrate

Table 4: Three Multilayer Selective Emitter Stacks Made of Al/Silica with Absorption Peak Around the Bandgap Wavelength of Three Converter Cell

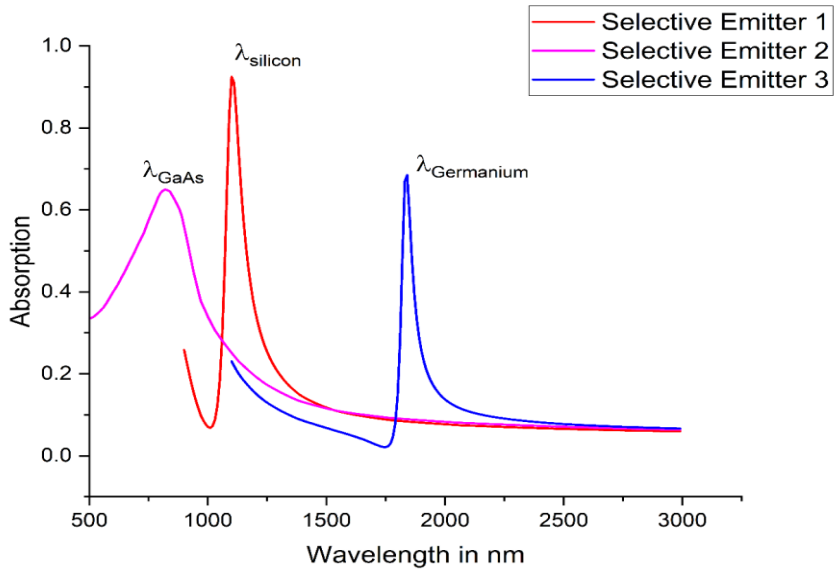

Figure 2: Absorption Peaks of the Three designed Selective Emitters Around Bandgap Wavelengths of Respective Converter Cells

These Al/Silica selective emitters, as mentioned before, are intended for medium-grade waste heat sources, as Al is limited by its melting point at about 933.5K.

Best Choice for Angle of Incidence According to Polarization

The absorption intensity at different wavelengths of the absorption spectrum was studied for different angles of incidence for different polarizations and depicted using color maps (Figure 3, Figure 4 and Figure 5). This was a crucial initial step in the design of the multilayer selective emitters, as it was then easy to understand how to get an absorption peak around the bandgap wavelength of the respective converter cell using these color maps. In the following color maps, selective emitter 1 from Table 4 is shown as an example.

The absorption intensity for selective emitter 1 is desired to be maximum around the bandgap wavelength of Si (around 1100nm). For all the three polarizations, this range is best obtained by normal angle of incidence (0 degrees). It is seen from the color maps that the absorption intensity for 0-degree angle of incidence is high around the bandgap wavelength of a Si cell, and minimum for other wavelength ranges of the absorption spectrum. Hence, to calculate the response of selective emitter 1, for example, unpolarized light at 0-degree angle of incidence was considered.

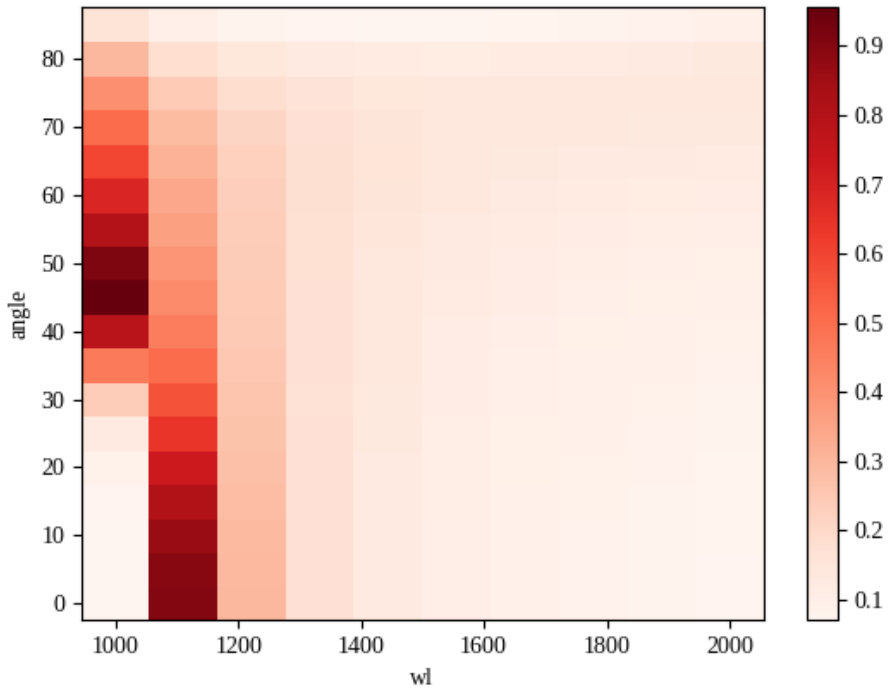

Figure 3: Color Map of the Absorption of Selective Emitter 1 for P Polarized Light

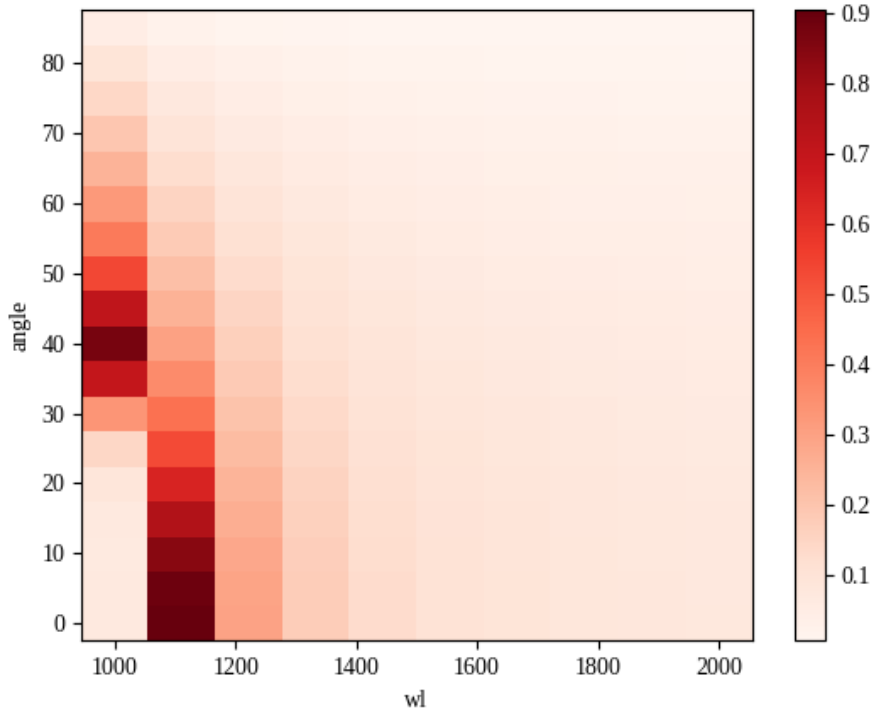

Figure 4: Color Map of The Absorption of Selective Emitter 1 for S Polarized Light

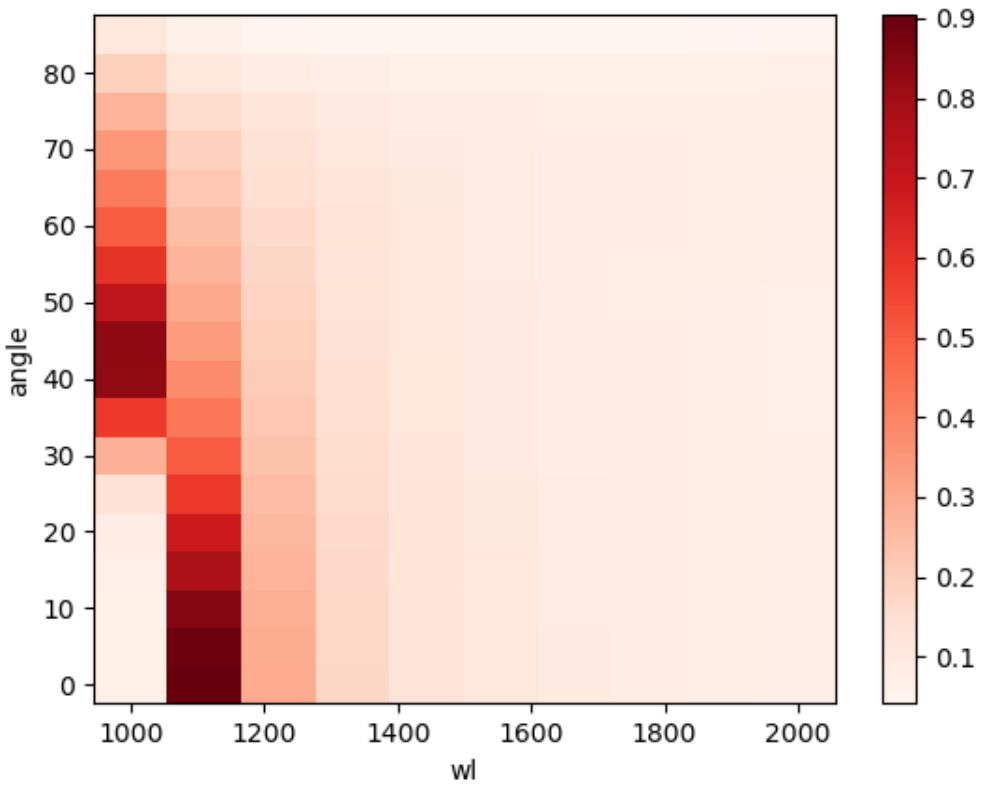

Figure 5: Color Map of the Absorption of Selective Emitter 1 for Unpolarized Light

Thickness Affects the Absorption Spectrum

In the initial stages of the design of the selective emitters, it was important to confirm that the thickness of the layers in a multilayer stack affects the absorption peak and intensity. As an example, selective emitter 1 listed in Table 4 is considered again. With reference to Figure 6, as the thickness of the Silica layer inside the cavity is increased, the absorption peak shifts towards longer wavelengths. As the thickness of the top metal layer is increased, the intensity of the absorption peak decreases and slightly shifts towards lower wavelengths.

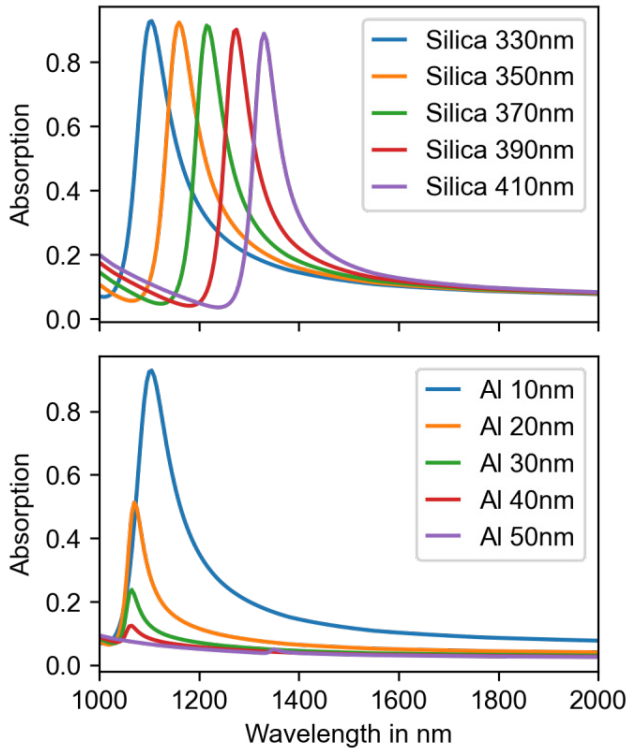

Figure 6: Thickness of the Middle Silica Layer and the Top Al Metal Layer Affects the Spectral Response

Absorption Coefficients of the Converter Cells as A Function of Wavelength Of The Incoming Radiation

The absorption coefficients of the materials for the converter cells considered in this research were calculated from the extinction coefficient values from the database (for Si, for Ge, for GaAs) using the relation [9-11]:

$$\alpha = 4\pi k/\lambda$$

Equation 1

where,

- k is the wavelength dependent extinction coefficient (cm-1)
- λ is the wavelength of the incident radiation (converted from μm to cm)

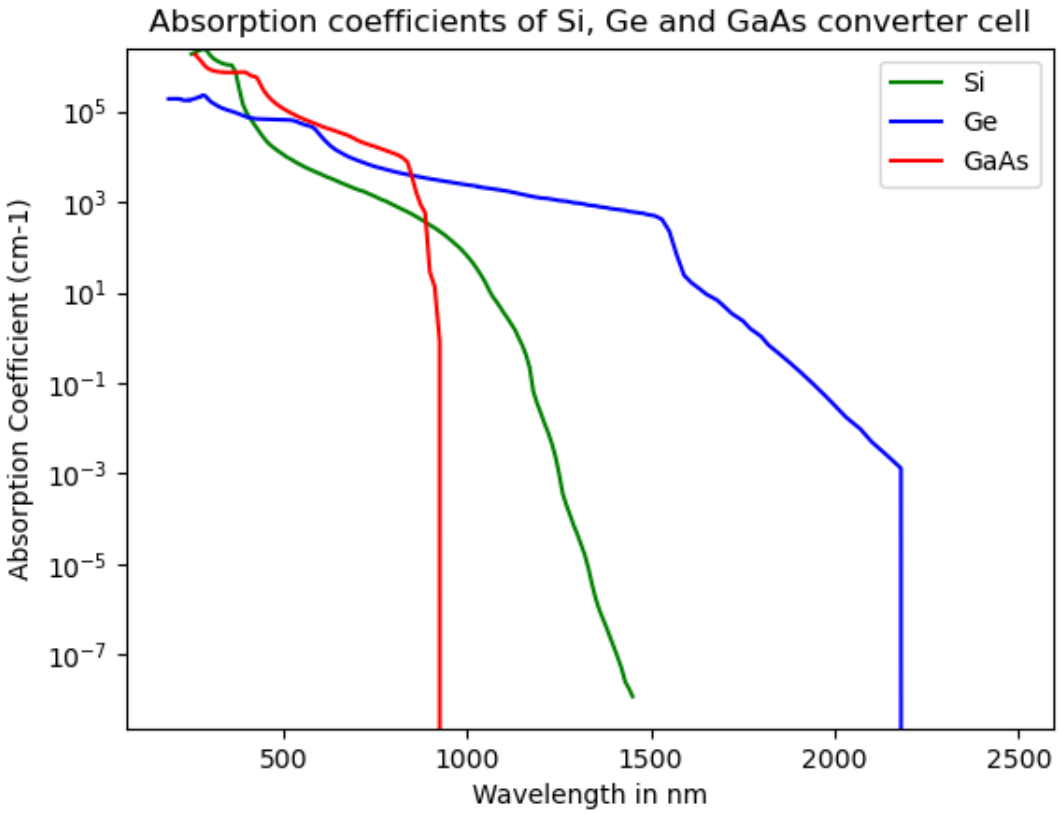

Figure 7: Calculated Absorption Coefficients of Si, Ge and GaAs Converter Cell as a Function of Wavelength of the Incident Radiation

Design of the P-N Junction Converter Cell

The spectral response calculations were done for a p-n junction converter cell illustrated in Figure 8.

For light to effectively reach the junction of a p-n junction in a converter cell, the junction needs to be positioned near the surface of the semiconductor. Additionally, the junction area must be sufficiently large to capture the desired radiation. This requirement leads to the necessity of having a thin n- or p-type junction on the side of the converter cell that is exposed to light.

This thin layer is required to be as conductive as possible. This can be achieved by heavy doping. Also, the mobility of the material affects its conductivity. Higher mobility means better conductivity. Since the electron mobility in a n type material is higher than the hole mobility in a p type material, the thin layer is taken as a highly-doped n type layer.

A thick p type region, as depicted in the Figure 8, absorbs almost all of the remaining radiation.

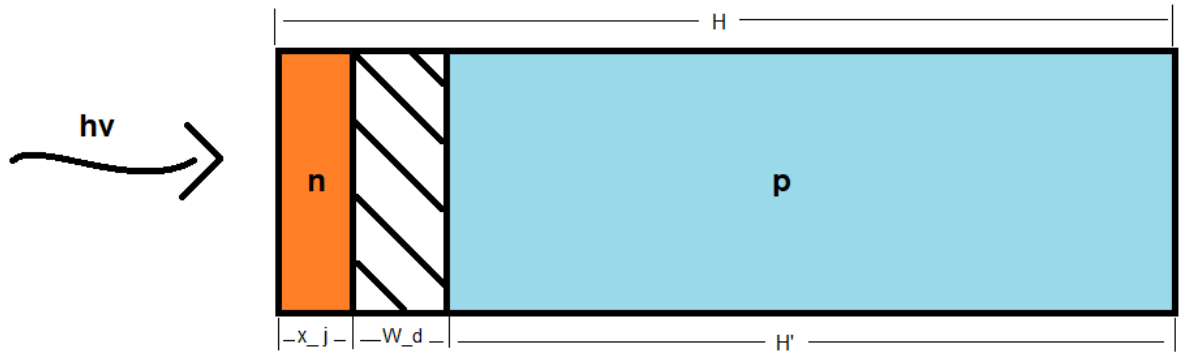

Figure 8: Schematic Illustration of the p-n Junction Converter Cell Considered in this Chapter

Calculation of the Depletion Layer Width (W_d)

The depletion layer width of a p-n junction device can be calculated using the equations based on semiconductor physics principles [12].The width of the depletion layer depends on the doping concentrations of the p-type and n-type regions, as well as the built-in potential (V_0) of the junction.

$$V_0 = k_B T/q \ln\left((N_a N_d)/(n_i^2)\right)$$

Equation 2

where:
- k_B is the Boltzmann constant (1.38×10^{-23} J/K),
- T is the absolute temperature in Kelvin (K),
- q is the elementary charge (1.6×10^{-19} C),
- N_a and Nd are the acceptor and donor doping concentrations, respectively (/cm^3),
- n_i is the intrinsic carrier concentration of the semiconductor at temperature T (/cm^3).

The following formula was used to calculate the width (W_d) of the depletion layer:

$$W_d = \sqrt{\frac{2\varepsilon_s V_0}{q}} \sqrt{\left(\frac{1}{N_a} + \frac{1}{N_d}\right)}$$

Equation 3

where:
- ε_s is the permittivity of the semiconductor (F/cm),
- q is the elementary charge (1.6×10^{-19} C),
- N_a and Nd are the acceptor and donor doping concentrations, respectively (/cm3),
- V_0 is the built-in potential of the p-n junction (V).

Calculations of Diffusion Coefficients and Diffusion Lengths (D_n, D_p, L_n and L_p)

These calculations offer critical understanding of how carriers are transported within a p-n junction solar cell and are crucial for optimizing device performance.

The diffusion coefficients, D_n and D_p for electrons and holes respectively, were calculated using the Einstein relation.

$$D_n = \frac{k_B T}{q} \mu_n$$

Equation 4

$$D_p = \frac{k_B T}{q} \mu_p$$

Equation 5

where:
-k_B is the Boltzmann's constant (1.38×10^{-23} J/K),
-q is the elementary charge (1.6×10^{-19} C),
-T in this research is the room temperature in Kelvin (K),
-μ_n and μ_p are the electron and hole mobilities respectively considered at room temperature.

The diffusion lengths, L_n and L_p for electrons and holes were calculated using the following relations.

$$L_n = \sqrt{D_n \tau_n}$$

Equation 6

$$L_p = \sqrt{D_p \tau_p}$$

Equation 7

where:
- τ_n and τ_p are the carrier lifetimes of electrons and holes respectively.

Spectral Response of The Converter Cells

Unlike Quantum Efficiency (QE) curves that exhibit a square shape, the spectral response of a semiconductor decreases at shorter wavelengths where each photon carries higher energy. This decrease in spectral response at shorter wavelengths occurs because the efficiency of converting photon energy to electrical current is less effective at these higher energies. The high-energy photons lead to significant surface recombination and a lower power-to-power ratio, which together cause the spectral response to drop. For a better understanding, one may refer to where the behavior of semiconductor devices under various conditions is well-explained [13].

Calculations of the Spectral Response

With reference to the formulae used for the calculation of the spectral response are summarized as below [14].

$$Spectral\ Response(\lambda) = \frac{J_L(\lambda)}{q\emptyset(\lambda)[1 - R(\lambda)]} = \frac{J_p(\lambda) + J_n(\lambda) + J_{dr}(\lambda)}{q\emptyset(\lambda)[1 - R(\lambda)]}$$

Equation 8

where:
• J_p is the photocurrent generated and collected in the front side of the converter cell,

$$J_p = [q\emptyset(1-R)\alpha L_p/(\alpha^2 L_p^2 - 1)] \times \left[\frac{\left(\frac{S_p L_p}{D_p} + \alpha L_p\right) - \exp(-\alpha x_j)\left(\frac{S_p L_p}{D_p}\cosh\frac{x_j}{L_p} + \sinh\frac{x_j}{L_p}\right)}{\frac{S_p L_p}{D_p}\sinh\frac{x_j}{L_p} + \cosh\frac{x_j}{L_p}} - \alpha L_p \exp(-\alpha x_j)\right]$$

Equation 9

• J_n is the electron photocurrent generated in the substrate of the cell,

$$J_n = \frac{q\emptyset(1-R)\alpha L_n}{\alpha^2 L_n^2 - 1}\exp\left[-\alpha\left(x_j + W_d\right)\right] \times \{\alpha L_n - \frac{(S_n L_n/D_n)\left[\cosh(H`/L_n) - \exp(-\alpha H`)\right] + \sinh(H`/L_n) + \alpha L_n \exp(-\alpha H`)}{(S_n L_n/D_n)\sinh(H`/L_n) + \cosh(H`/L_n)}\}$$

Equation 10

• J_{dr} is the photocurrent generated within the depletion region,

$$J_{dr} = q\emptyset(1-R)\exp\left(-\alpha x_j\right)[1 - \exp(-\alpha W_D)]$$

Equation 11

• J_L is the total photocurrent.

where,
• α(λ) is the wavelength dependent absorption coefficient (cm^{-1})
• L_p is the diffusion length of holes (cm)
• D_p is the diffusion coefficient of holes (cm^2/s)
• S_p is the surface recombination velocity (cm/s)
• x_j is the thickness of the n layer (cm)
• φ(λ) is the number of incident photons per area per time per unit bandwidth
• R(λ) is the fraction of the photons reflected from the surface
• L_n is the diffusion length of electrons (cm)
• D_n is the diffusion coefficient of electrons (cm^2/s)
• S_n is the back-surface recombination velocity (cm/s)
• H` is the thickness of the p substrate minus the depletion layer (cm)
• W_d is the depletion layer width (cm)

The spectral response of the three converter cells – Si, Ge and GaAs – was calculated and plotted against the wavelength of the incident photons as shown in the plots that follow. The effect of the surface recombination velocity was also plotted for each converter cell. For best spectral response of the TPV cells at all wavelengths, it is seen that the surface recombination velocity must be low. By limiting the surface recombination, the minority carrier lifetime is increased (because minority carriers are depleted slowly towards the front contact/surface). Longer minority carrier lifetime means better efficiency of a TPV cell.

By implementing techniques such as hydrogen passivation and anti-reflection coatings, in combination or individually, surface recombination velocity can be efficiently lowered.

Spectral Response of Si Converter Cell

N_a	1.5e16 /cm^3 [14]
N_d	5e19 /cm^3 [14]
D_n (for Substrate)	Calculated 35.1 cm^2/s
D_p (for Front)	Calculated 12.48 cm^2/s
τ_n (for Substrate)	10 µs [14]
τ_p (for Front)	0.5 µs [14]
L_n (for Substrate)	Calculated 0.01873 cm
L_p (for Front)	Calculated 0.00223 cm
S_n (for Substrate)	10^6 cm/s [14]
S_p (for Front)	Determined 10^5 cm/s
x_j (for Front)	5e-5 cm [14]
W_d (for Depletion Layer)	Calculated 2.6586e-5 cm
H' (for Substrate)	Calculated 0.044923 cm
H (total Width)	0.045 cm [14]

Table 5: Overview of Parameters Considered for the Calculation of Spectral Response of a Si Converter Cell

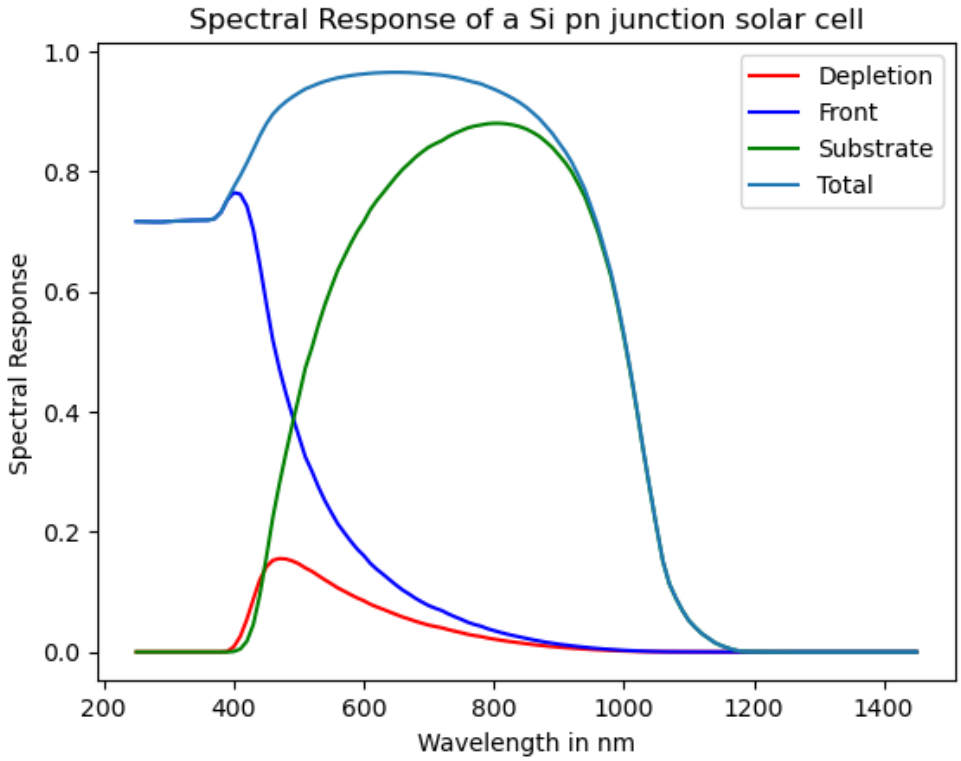

Figure 9: Calculated Spectral Response of a Si p-n Junction Converter Cell

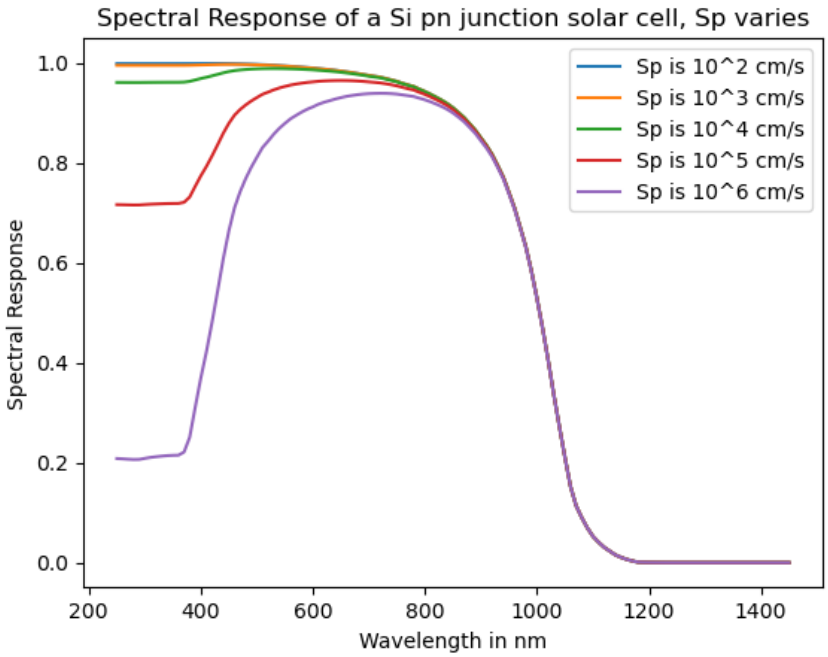

Figure 10: Computed Internal Spectral Response of a Si p-n Junction Converter Cell with Different Surface Recombination Velocities

Spectral Response of Ge Converter Cell

N_a	1e19/cm^3
N_d	1e17/cm^3
D_n (for Substrate)	101.39 Calculated cm^2/s
D_p (for Front)	49.4 Calculated cm^2/s
τ_n (for Substrate)	2 µs
τ_p (for Front)	2 µs
L_n (for Substrate)	Calculated 0.0142 cm
L_p (for Front)	Calculated 0.00993 cm
S_n (for Substrate)	10^9 cm/s
S_p (for Front)	10^5 cm/s
x_j (for Front)	5e-5 cm [14]
W_d (for Depletion Layer)	Calculated 8.75e-6 cm
H' (for Substrate)	Calculated 0.044941 cm
H (total Width)	0.045 cm [14]

Table 6: Overview of Parameters Considered for the Calculation of spectral Response of a Ge Converter Cell

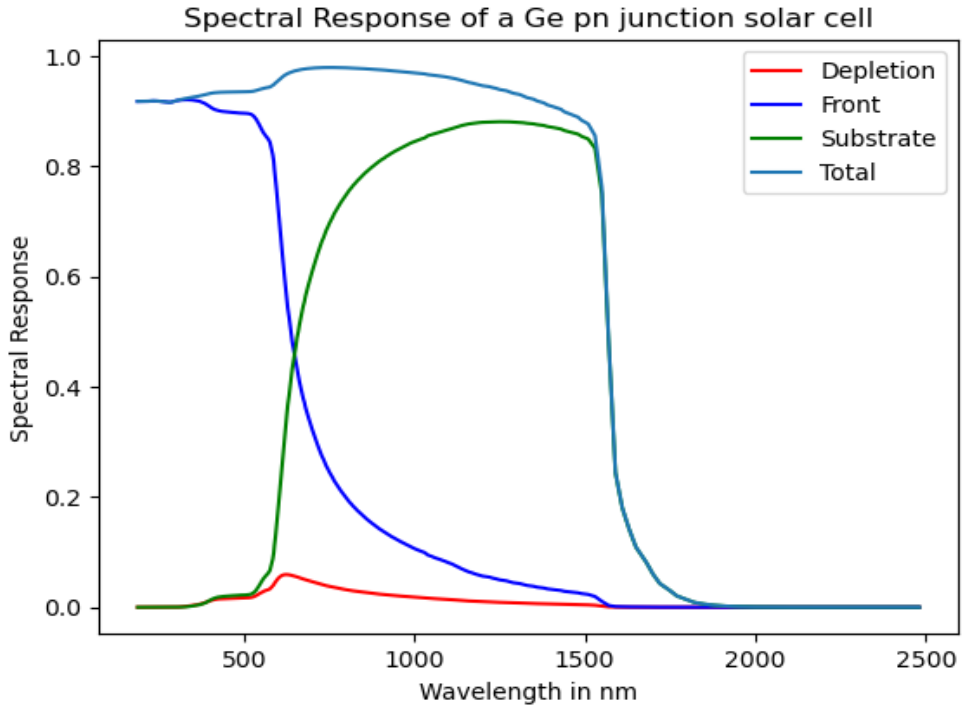

Figure 11: Calculated Spectral Response of a Ge p-n junction converter cell

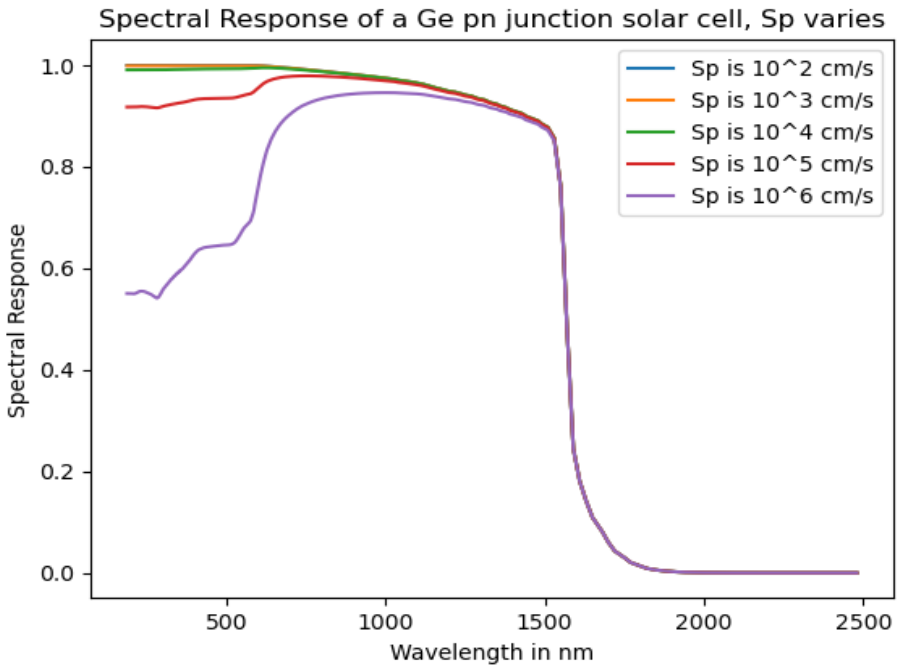

Figure 12: Computed Internal Spectral Response of a Ge p-n Junction Converter Cell with Different Surface Recombination Velocities

Spectral Response of GaAs Converter Cell

N_a	1e19/cm^3
N_d	1e17/cm^3
D_n (for Substrate)	Calculated 221 cm^2/s
D_p (for Front)	Calculated 10.4 cm^2/s
τ_n (for Substrate)	2 µs
τ_p (for Front)	2 µs
L_n (for Substrate)	Calculated 0.021 cm
L_p (for Front)	Calculated 0.00456 cm
S_n (for Substrate)	10^9 cm/s
S_p (for Front)	10^5 cm/s
x_j (for Front)	5e-5 cm [14]
W_d (for Depletion Layer)	Calculated 1.1423e-5 cm
H' (for Substrate)	Calculated 0.04493 cm
H (total Width)	0.045 cm [14]

Table 7: Overview of Parameters Considered for the Calculation of Spectral Response of a GaAs Converter Cell

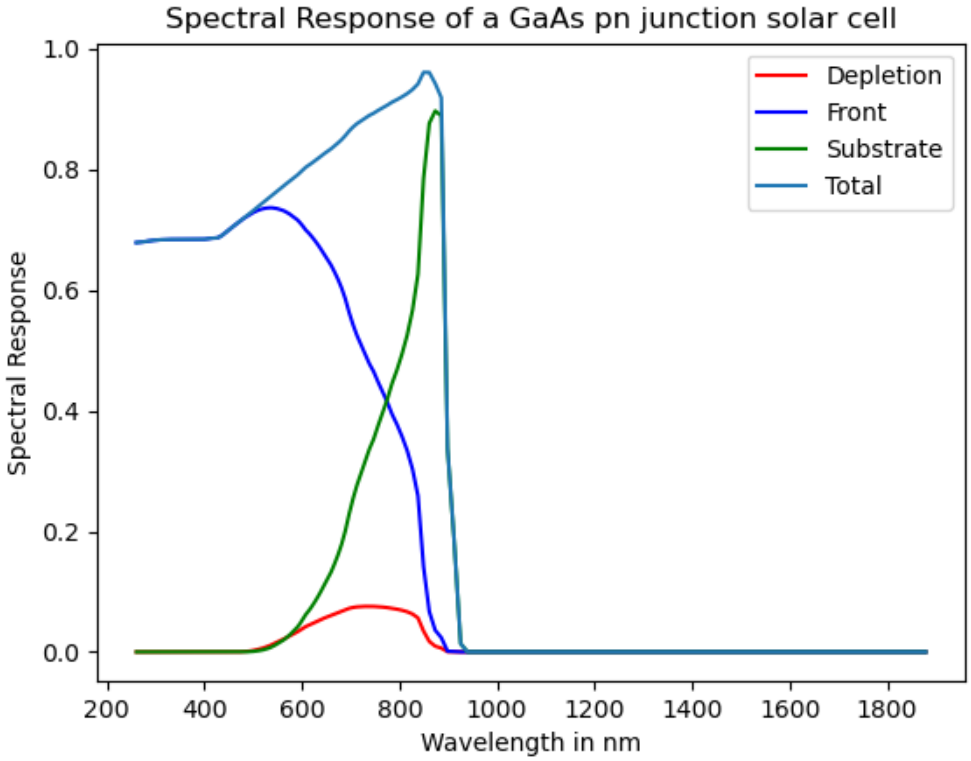

Figure 13: Calculated Spectral Response of a GaAs p-n Junction Converter Cell

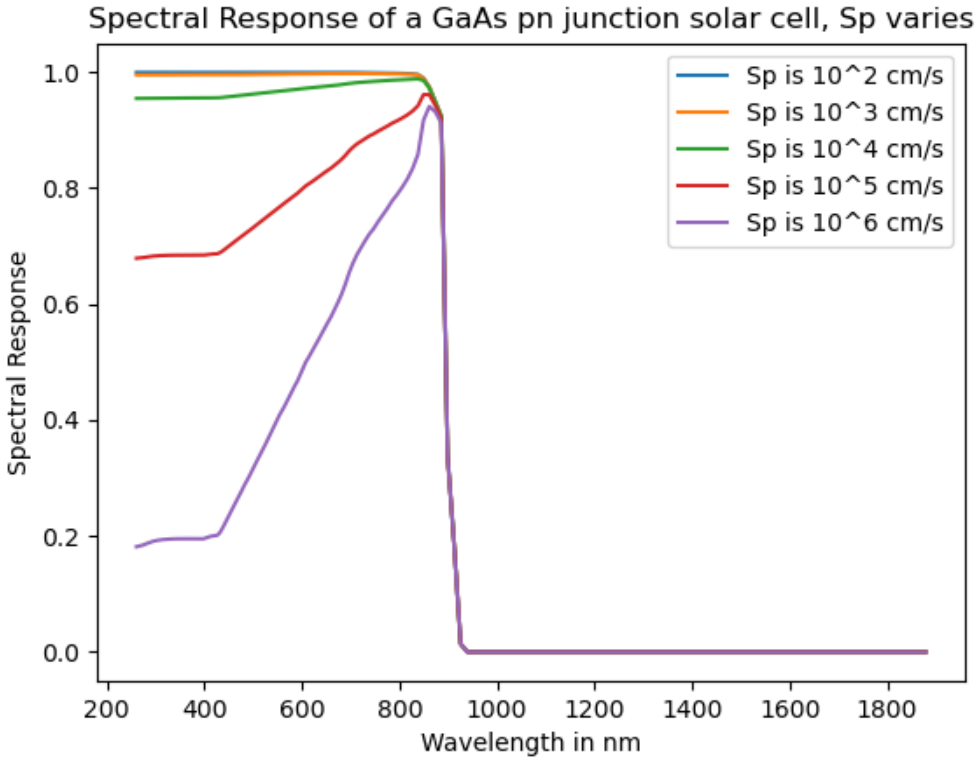

Figure 14: Computed Internal Spectral Response of a GaAs p-n Junction Converter Cell with Different Surface Recombination Velocities

Conclusion

In this comprehensive study, multilayer selective emitters were meticulously examined using the TMM algorithm. These emitters were intended to operate effectively within the infrared spectrum, matching the operational wavelengths of TPV systems. By manipulating the thickness and material composition of each layer, the emitters were fine-tuned to maximize absorption (and thus emissivity) at desired wavelengths while minimizing losses at others.

The focus on the absorption spectrum of these multilayers is rooted in Kirchhoff's law of thermal radiation. By studying the absorption spectrum, one can infer the emission characteristics of the selective emitter, making this approach both efficient and insightful.

The main analysis of this study was the design of three aluminum and silica based selective emitters intended for TPV systems. These designs were evaluated to determine their effectiveness in converting thermal energy to electrical energy, a critical aspect for optimizing TPV systems.

In summary, the study of multilayer selective emitters using the TMM algorithm has provided valuable insights into their design and optimization for TPV systems. The applicability of these emitters to medium-grade heat sources in various industries underscores their potential to contribute significantly to energy efficiency and sustainability.

The spectral response of three p-n junctions analyzed their ability to perform as good converter cells in a thermophotovoltaic system.

References

1. Atak, E. E. (2021). Investigation of Nanostructured Surfaces for Thermophotovoltaic Applications (Master's thesis, Middle East Technical University (Turkey))
2. Pfiester, N. A., & Vandervelde, T. E. (2017). Selective emitters for thermophotovoltaic applications. *Physica status solidi (a), 214*(1), 1600410.
3. Datas, A., & Vaillon, R. (2019). Thermionic-enhanced near-field thermophotovoltaics for medium-grade heat sources. *Applied Physics Letters, 114*(13).
4. S. Byrnes, "Tmm package" [Accessed June 2023].
5. S. J. Byrnes, "Multilayer optical calculations," arXiv: Computational Physics 1603.02720, 2016. [Online].
6. Ordal, M. A., Bell, R. J., Alexander Jr, R. W., Newquist, L. A., & Querry, M. R. (1988). Optical properties of Al, Fe, Ti, Ta, W, and Mo at submillimeter wavelengths. *Applied optics, 27*(6), 1203-1209.
7. McPeak, K. M., Jayanti, S. V., Kress, S. J., Meyer, S., Iotti, S., Rossinelli, A., & Norris, D. J. (2015). Plasmonic films can easily be better: rules and recipes. *ACS photonics, 2*(3), 326-333.
8. Johnson, P. B., & Christy, R. W. (1972). Optical constants of the noble metals. *Physical review B, 6*(12), 4370.
9. https://www.pvlighthouse.com.au/refractive-index-library
10. Nunley, T. N., Fernando, N. S., Samarasingha, N., Moya, J. M., Nelson, C. M., Medina, A. A., & Zollner, S. (2016). Optical constants of germanium and thermally grown germanium dioxide from 0.5 to 6.6 eV via a multisample ellipsometry investigation. *Journal of Vacuum Science & Technology B, 34*(6).
11. Papatryfonos, K., Angelova, T., Brimont, A., Reid, B., Guldin, S., Smith, P. R., ... & Selviah, D. R. (2021). Refractive indices of MBE-grown AlxGa (1− x) As ternary alloys in the transparent wavelength region. *AIP Advances, 11*(2).
12. Kitai, A. (2011). Principles of Solar Cells, LEDs and Diodes: The role of the PN junction. John Wiley & Sons.
13. Pierret, R. F. (1996). Semiconductor device fundamentals. Pearson Education India.
14. Sze, S. M., & Ng, K. K. (2007). Photodetectors and solar cells. *Physics of semiconductor devices, 13,* 667-683.